Climatology and Interannual Variability of Boreal Spring Wet Season Precipitation in the Eastern Horn of Africa and Implications for Its Recent Decline

BRANT LIEBMANN,[a,b] ILEANA BLADÉ,[c] CHRIS FUNK,[d,e] DAVE ALLURED,[a,b] XIAO-WEI QUAN,[a,b] MARTIN HOERLING,[b] ANDREW HOELL,[b] PETE PETERSON,[e] AND WASSILA M. THIAW[f]

[a] *CIRES, University of Colorado Boulder, Boulder, Colorado*
[b] *Physical Sciences Division, NOAA/Earth System Research Laboratory, Boulder, Colorado*
[c] *Grup de Meteorologia, Departament de Física Aplicada, Universitat de Barcelona, Barcelona, Spain*
[d] *U.S. Geological Survey, Earth Resources Observation and Science Center, Sioux Falls, South Dakota*
[e] *Climate Hazards Group, Department of Geography, University of California, Santa Barbara, Santa Barbara, California*
[f] *Climate Prediction Center, NOAA/National Centers for Environmental Prediction, Camp Springs, Maryland*

(Manuscript received 14 June 2016, in final form 31 January 2017)

ABSTRACT

The 1981–2014 climatology and variability of the March–May eastern Horn of Africa boreal spring wet season are examined using precipitation, upper- and lower-level winds, low-level specific humidity, and convective available potential energy (CAPE), with the aim of better understanding the establishment of the wet season and the cause of the recent observed decline. At 850 mb, the development of the wet season is characterized by increasing specific humidity and winds that veer from northeasterly in February to southerly in June and advect moisture into the region, in agreement with an earlier study. Equally important, however, is a substantial weakening of the 200-mb climatological easterly winds in March. Likewise, the shutdown of the wet season coincides with the return of strong easterly winds in June. Similar changes are seen in the daily evolution of specific humidity and 200-mb wind when composited relative to the interannual wet season onset and end, with the easterlies decreasing (increasing) several days prior to the start (end) of the wet season. The 1981–2014 decrease in March–May precipitation has also coincided with an increase in 200-mb easterly winds, with no attendant change in specific humidity, leading to the conclusion that, while high values of specific humidity are an important ingredient of the wet season, the recent observed precipitation decline has resulted mostly from a strengthening of the 200-mb easterlies. This change in the easterly winds appears to be related to an increase in convection over the Indonesian region and in the associated outflow from that enhanced heat source.

1. Introduction

Understanding the mechanisms driving precipitation variability and change in the Horn of Africa is a pressing matter. Local agriculture is primarily rain fed (e.g., Mati 2005), and rainfall amounts have always been too variable to allow for consistent ''food security'' (Funk et al. 2008). Any future changes in precipitation totals, and/or in their temporal and spatial distribution, would further threaten food security, a situation compounded by alterations in land use and population growth (e.g., Maltima et al. 2009).

The low-lying eastern Horn of Africa region is singular in several respects. First, as shown in Fig. 1a, the region is almost completely cut off from the rest of the continent by a ring of mountains that includes some of Africa's tallest peaks and is broken only by the Turkana Valley in northwestern Kenya. Second, the region is arid to semiarid, in stark contrast with the rest of near-equatorial Africa (e.g., Nicholson 1996). Last, the precipitation regime is characterized by two distinct wet seasons, even in its northern section located well north of the equator; elsewhere at this latitude (~10°N), rainfall occurs almost entirely as a single wet season during June–September. The distinctive precipitation regime and orography of the Horn of Africa region are related in ways that involve multiple processes, such as orographic blocking of low-level moisture flows, ocean–atmospheric interactions, and ocean upwelling, and are not fully understood (Nicholson and Entekhabi 1987; Nicholson 1996; Slingo et al. 2005). In fact, even the precise reasons for the

Corresponding author e-mail: Ileana Bladé, ileanablade@ub.edu

DOI: 10.1175/JCLI-D-16-0452.1

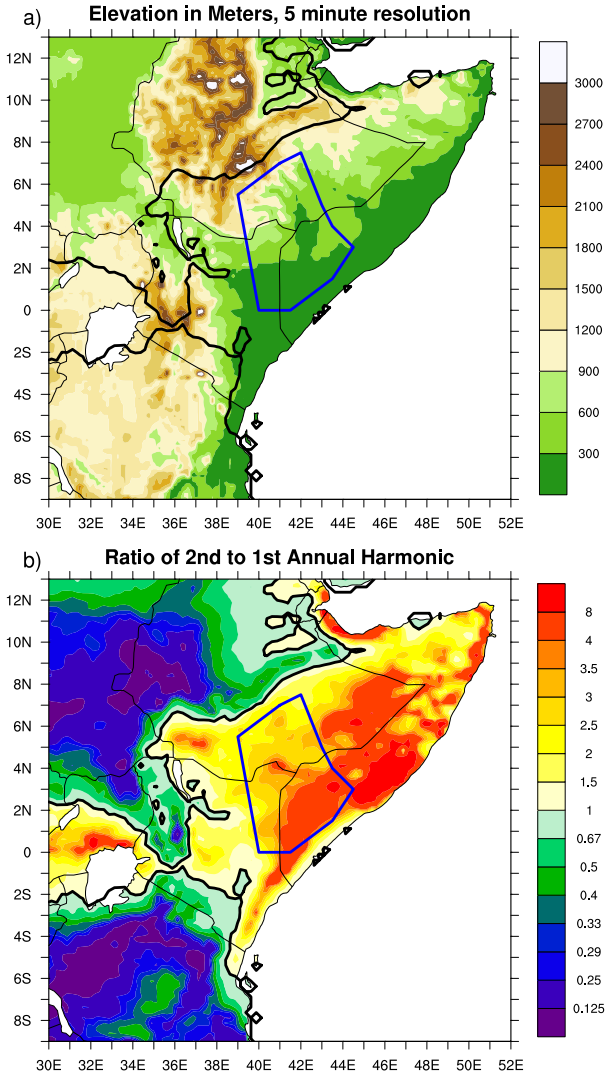

FIG. 1. (a) Elevation in meters. (b) Ratio of the second to first harmonic of monthly precipitation climatology for 1981–2014. Black contour in both panels indicates that the ratio of the second to first annual harmonic is equal to 1. Blue polygon indicates region over which data are averaged in subsequent analysis.

existence of two separate rainy seasons are not clear (e.g., Nicholson 1996).

The unique character of the seasonal cycle of precipitation in the Horn region is illustrated in Fig. 1b, which shows the ratio of the second to first harmonic of eastern Africa precipitation (data to be detailed subsequently) and reveals a dominant second harmonic almost exclusively over the eastern Horn region, consistent with many previous reports of two wet seasons there (e.g., Nicholson 1996; Hastenrath et al. 2007; Liebmann et al. 2012; Yang et al. 2015). These two rainy seasons are referred to as the short rains of October–December (OND) and the long rains of March–May (MAM). In addition to the Horn region, there is a small region in the western sector, right on the equator, in which the second harmonic is also large. This regime, however, is part of a zonally wide, but latitudinally narrow, near-equatorial region in which two equinoctial wet seasons occur associated with the biannual crossing of the sun over the equator (e.g., Liebmann et al. 2012, their Fig. 6). This is in contrast to the Horn region, whose double wet season is not related to the two zenith passages of the sun, as evident from both its geographical location and the delayed timing relative to the equinoxes (e.g., Nicholson 1996).

The "short rain" season is the better understood of the two seasons with regard to its interannual variability at least (e.g., Hastenrath et al. 2007, 2011). It is well established, for instance, that short-rain precipitation totals exhibit a strong positive relationship with both El Niño (e.g., Ogallo et al. 1988; Kiladis and Diaz 1989; Hutchinson 1992; Indeje et al. 2000; Mason and Goddard 2001) and the Indian Ocean dipole (Saji et al. 1999). The focus of this paper, however, is the poorly understood "long rain" and primary growing season of the eastern Horn, active roughly from March through May. Rainfall in this season is not well correlated with any known mode of SST variability, and successful seasonal prediction of precipitation based on empirically derived relationships, from either observations or output from coupled ocean–atmosphere models, has proved elusive (e.g., Ogallo et al. 1988; Indeje et al. 2000; Camberlin and Philippon 2002; Camberlin and Okoola 2003). Yet the long-rain season is of current interest because several studies have reported a substantial decline in precipitation in the last approximately 30 years (Funk et al. 2005, 2008; Williams and Funk 2011; Lyon and DeWitt 2012; Hoell and Funk 2014; Liebmann et al. 2014; Maidment et al. 2015; Hoell et al. 2017), spurring substantial research into its causes (e.g., Williams and Funk 2011; Lyon and DeWitt 2012; Lott et al. 2013; Liebmann et al. 2014). Moreover, Tierney et al. (2015) infer from proxy evidence that aridity in the Horn of Africa increased during the twentieth century at a rate that is "unusual" compared to the last 2000 years and argue that the signal could be dominated by a reduction in the long rains, consistent with the recent observed decrease.

One suggested explanation for the decreasing long rains involves an intensification of the Indian branch of the Walker circulation (Verdin et al. 2005; Funk et al. 2008; Williams and Funk 2011; Lyon and DeWitt 2012; Lyon 2014; Lyon et al. 2014; Funk and Hoell 2015). According to this view, the recent observed warming in the warm pool region (e.g., Hartmann et al. 2013) has increased convection over Indonesia and strengthened the Indian Ocean upper-level easterlies emanating from

this convective area, thereby inducing anomalous upper-level convergence and reduced rainfall over the Horn, where climatological subsidence already prevails (Yang et al. 2015). Evidence for the validity of this hypothesis has been provided by AMIP-type model simulations that reproduce the observed MAM precipitation decrease when forced with the recent history of SST anomalies (e.g., Lyon and DeWitt 2012; Liebmann et al. 2014; Lyon 2014; Lyon et al. 2014; Yang et al. 2014). In particular, Liebmann et al.'s (2014) ECHAM5 34-member ensemble exhibited a drying trend in almost every individual run, suggesting that the Walker cell mechanism could explain at least some of the observed drying in the Horn region. Even though confidence in that finding is diminished by the absence of a consistent long-term interannual relationship between observed MAM Horn precipitation and equatorial SSTs (anywhere), when the analysis is restricted to the most recent 1996–2012 period a correlation pattern emerges that is quite similar to that found in the ECHAM5 ensemble. This suggests that the coupling has become stronger of late, although it is difficult to establish statistical significance when the length of record is short and arbitrarily chosen (Liebmann et al. 2014).

A further caveat for the Walker cell argument is that the evidence for an Indian Ocean Walker cell extending all the way to the Horn region is limited. In fact, even for the equatorial strip, Hastenrath (2000) found a closed zonal circulation to be present only in boreal autumn (October). However, subsidence does prevail over the Horn year-round, even in MAM (albeit weak), and this subsidence could be modulated by Indian Ocean upper-level easterlies and/or Indonesian convection even in the absence of a closed zonal circulation.

Complicating this issue, seasonal precipitation in the eastern Horn, as in any other location, is not a continuous event over a fixed length period. Changes in seasonal totals may reflect variations in both onset and end dates, as well as rain rate or number of rainy days within the season. It is currently unclear which aspect of the long rains is typically more altered during failed rainy seasons and whether the recent increase in the frequency of droughts may be understood as a mere weakening of the seasonal cycle or rather as a change in the atmospheric thermal conditions, circulation, or moisture budget. As already mentioned, the annual cycle of precipitation in the Horn is itself poorly understood, including fundamental questions such as the reason for the bimodal annual cycle and the differences in dynamics and thermodynamics between the two wet seasons. Progress in understanding the recent decline in long rains then requires delving into the climatological properties of this wet season.

In a recent paper, Yang et al. (2015, hereafter Y15) examined the annual cycle of eastern Horn precipitation. They found that the atmosphere is conditionally stable in all seasons, but least stable during MAM, and that the annual cycle of this conditional instability is dominated by variations in the surface moisture advected from the east, since the mountains to the west block the flux of moist air from that direction. They then argued that the existence of two separate spring and autumn wet seasons, with suppressed rainfall in between, could be understood in terms of the annual cycle of surface monsoonal winds and Indian Ocean SSTs. During the dry seasons, strong alongshore low-level winds advect dry air from the winter hemisphere, where SSTs are relatively cold, into the Horn region. This is particularly true in boreal summer when the monsoon-related northward Findlater or Somali jet (Findlater 1969) drives strong coastal cooling via evaporation, upwelling, and entrainment (McCreary et al. 1993). In the interim seasons, the winds are weaker but more directly onshore and the off-coast Indian Ocean waters are much warmer, especially in MAM.

The purpose of this paper is to better understand regional-scale causes of the eastern Horn's long rains and their interannual and long-term variability, thus extending the work of Y15. In contrast with that paper, month-to-month changes in the climatology are examined here in order to more precisely identify the circulation changes that accompany the onset and demise of this wet season. Daily data are also used to spatially track the development and evolution of the wet season. Our findings show the existence of abrupt changes in the low-level moisture field and in the upper-level zonal winds associated with onset and end of the wet season. The importance of low-level moisture changes has been previously emphasized by Y15, but in this paper we provide new evidence that precipitation is also modulated by changes in the upper-level easterly winds, with precipitation commencing when the easterlies halt and ending when they resume. This relationship holds for both monthly climatologies and daily composites of wet season onset and end. Additionally, we show that the observed recent decrease in seasonal MAM total precipitation (last 34 yr) has also coincided with long-term seasonal increases in upper-level easterlies, unlike the attendant changes in the moisture field, which are relatively modest within the area in question.

2. Data and methods

Precipitation estimates used in this study are primarily from the Climate Hazards Group Infrared Precipitation with Stations (CHIRPS; Funk et al. 2015b) dataset. This product is a blend of Climate Hazards Group precipitation climatology (Funk et al. 2015a), satellite infrared measurements, and direct rain gauge measurements (which are

quite sparse over the eastern Horn of Africa). This study employs the 0.05° version for the period 1981–2014. Monthly TRMM (Kummerow et al. 1998) precipitation estimates (1998–2011) are used in one figure to show monthly climatologies that include the ocean, as well as outgoing longwave radiation (OLR) to estimate the large-scale change in precipitation (Liebmann and Smith 1996).

Gridded variables used to describe the atmospheric circulation and thermodynamical state were derived from the European Centre for Medium-Range Weather Forecasts (ECMWF) interim reanalysis (ERA-Interim; ECMWF 2009). Wind, specific humidity, divergence, omega velocity, precipitation, and convective available potential energy (CAPE) are represented on a 0.7° × 0.7° grid. CAPE is defined following the AMS Glossary of Meteorology as ''the maximum energy available to an ascending parcel'' (AMS 2012).

Onset and end of the wet season are determined by an objective, straightforward method already used in several previous studies of monsoonal rains (e.g., Liebmann and Marengo 2001; Liebmann et al. 2012; Dunning et al. 2016), and the description below derives from Liebmann and Marengo (2001) with minor modifications. This method compares well with other, agriculture-based definitions (Dunning et al. 2016) and, importantly, allows for the possibility of false onsets. For each time series (in the present case, at an individual grid point or for an average over several), the average annual precipitation total is computed and divided by 365 to obtain the mean daily climatological amount. For all years, starting at a chosen point in time, observed precipitation minus this daily climatology is summed. Onset is defined as the day on which the accumulated quantity is at an absolute minimum since after that date precipitation exceeds climatology. In this way, if a dry spell after an initial wet period is long enough that the anomalous accumulation dips below the value at the start of that wet period, that initial wet period would be considered a false onset. Similarly, the end of the wet season is defined as the day on which the summed quantity is at a maximum. For the present study, whose focus is on one of the two wet seasons of the Horn of Africa, the search begins on 1 January, well before the start of the wet season of interest. The rain rate is calculated simply as the amount of rain during a particular wet season divided by its length.

3. Results

a. *Climatology of the long rains*

Figure 2 shows climatologies of TRMM (1998–2011 average) precipitation (note nonlinear shading interval) and 200-mb (1 mb = 1 hPa) vector winds over Africa, the Indian Ocean, and beyond, for months surrounding the long rains. In February (Fig. 2a), tropical precipitation is centered slightly south of the equator over the western Pacific and Indian Oceans. The Horn of Africa is almost completely dry. The strongest winds reside in the Northern Hemisphere subtropics and midlatitudes, but winds exceeding $8\,\mathrm{m\,s^{-1}}$ with a large easterly and a smaller cross-equatorial component are evident along the equator over Africa and across the Indian Ocean. Cross-equatorial winds with a strong easterly component on the equatorward side of a large convective heat source (here, located in the Southern Hemisphere) are consistent with the solution of the linear shallow-water equations on a beta plane for a stationary off-equatorial heat source (Gill 1980)—as first proposed in Verdin et al. (2005) and further elaborated upon in Funk et al. (2008).

Of the changes that occur from February to March (Fig. 2b), the most relevant to the present analysis is a weakening of the easterlies and a decrease in precipitation over the western and central Indian Ocean, simultaneous with the onset of the wet season over the Horn. April precipitation (Fig. 2c) over Indonesia is similar to March, but it weakens further over the western Indian Ocean and moves northward over Africa and into the Horn, marking the peak of the wet season in this region. There is a more dramatic change from April to May (Fig. 2d) in the eastern Indian Ocean and Indonesia, when precipitation jumps northward, retreating from the Southern Hemisphere (e.g., Australia becomes almost completely dry) and greatly increasing over the Asian monsoon region. Precipitation over the Horn decreases as equatorial easterlies begin to develop again over the Indian Ocean, on the equatorward side of the now Northern Hemisphere heat source (also consistent with Gill 1980).

Large changes again occur from May to June (Fig. 2e). Precipitation increases substantially in the Northern Hemisphere east of about 60°E, primarily as a jump along the west coasts of Asia and to the west of India and Southeast Asia. Precipitation in central equatorial Africa moves slightly northward as well, as does the subtropical westerly jet. Most directly relevant to the Horn of Africa region is the pronounced increase in near-equatorial easterlies over the Indian Ocean and Africa. These winds may be viewed as the southern limb of the large-scale anticyclone that develops in response to the onset of the Asian summer monsoon. The Northern Hemisphere expansion of precipitation continues in July (Fig. 2f) and August (not shown), when African monsoonal precipitation is also at its maximum northward extent.

Figure 3 shows CHIRPS precipitation and a more detailed 200-mb wind climatology within the Horn

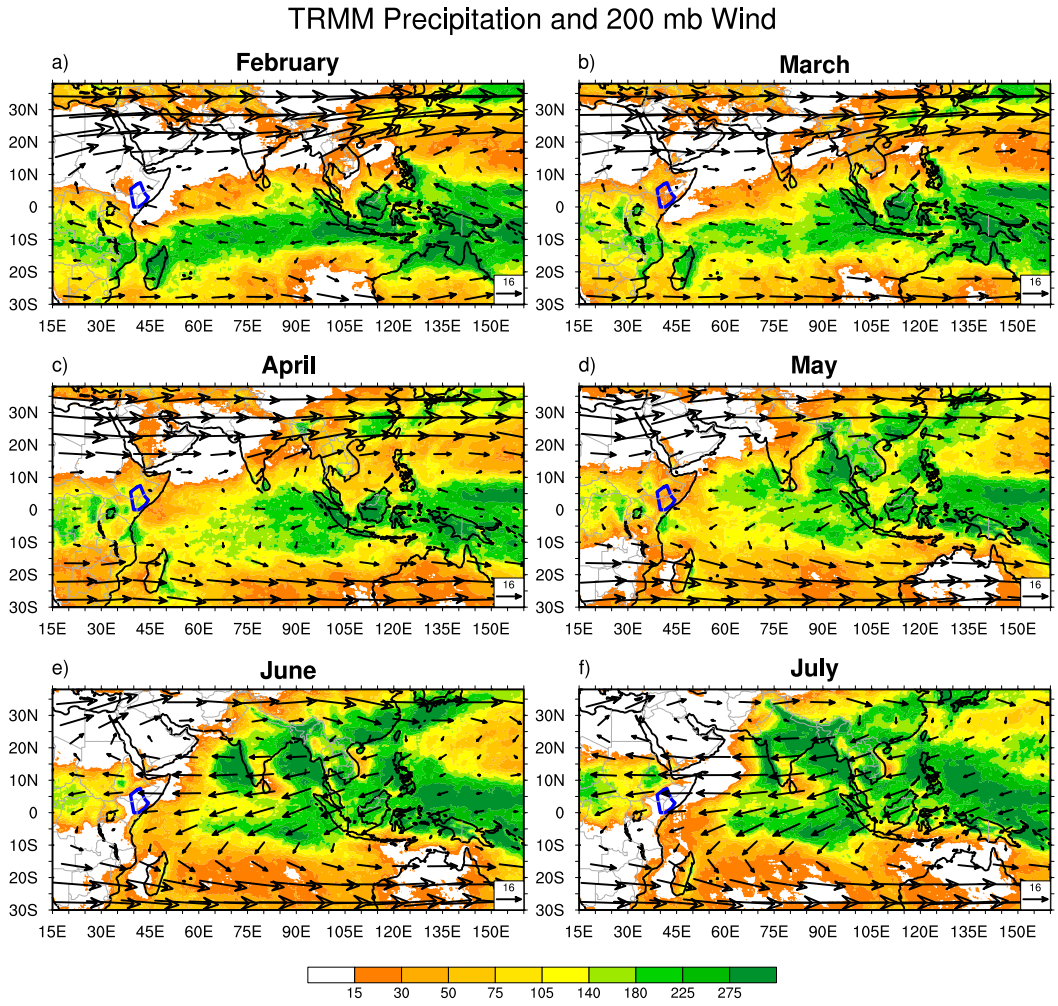

FIG. 2. Average monthly total precipitation (mm) estimated from TRMM (1998–2011; note uneven contour intervals) and 200-mb winds ($m\,s^{-1}$; reference vector in lower right of each map). Wind vectors are plotted every 8th grid point in latitude and 16th grid point in longitude. Vectors are omitted at grid points with speeds less than $1\,m\,s^{-1}$. Blue polygon over eastern Horn of Africa indicates region over which data are averaged in subsequent analysis.

domain, for the same months. February (Fig. 3a) is dry almost everywhere north of the equator, with strong easterlies over the ocean and southeasterly winds over land south of 4°N that turn into westerlies in the far north. March (Fig. 3b) signals the beginning of the primary wet season, with clear rainfall increases relative to February over most of the southern domain and the highlands of southwest Ethiopia. Winds over the eastern Horn and western Indian Ocean have slackened. By April (Fig. 3c) precipitation has intensified everywhere, making this month the wettest over the Horn, with amounts comparable to those at the same latitude in central Africa (Fig. 2c). The upper-level winds are weak over the entire domain (vectors weaker than $1\,m\,s^{-1}$ are not plotted). In May (Fig. 3d) precipitation decreases over the southern Horn and increases to the north, while easterlies make a weak reappearance (more visible over the ocean). Fully developed easterlies prevail throughout the area in June and July (Figs. 3e,f), as the eastern Horn becomes quite dry again (except in a narrow strip along the southern equatorial coast). Meanwhile, rain continues to increase over western Ethiopia.

We now turn our attention to the monthly climatology of 925-mb specific humidity and winds, shown in Fig. 4. In February (Fig. 4a) the low-level air is almost uniformly dry north of about 2°N, with a strong gradient perpendicular to the coast directed toward the ocean. The winds over the ocean are from the northeast and nearly parallel to isolines of humidity, thus advecting little moisture onto land, consistent with the results of

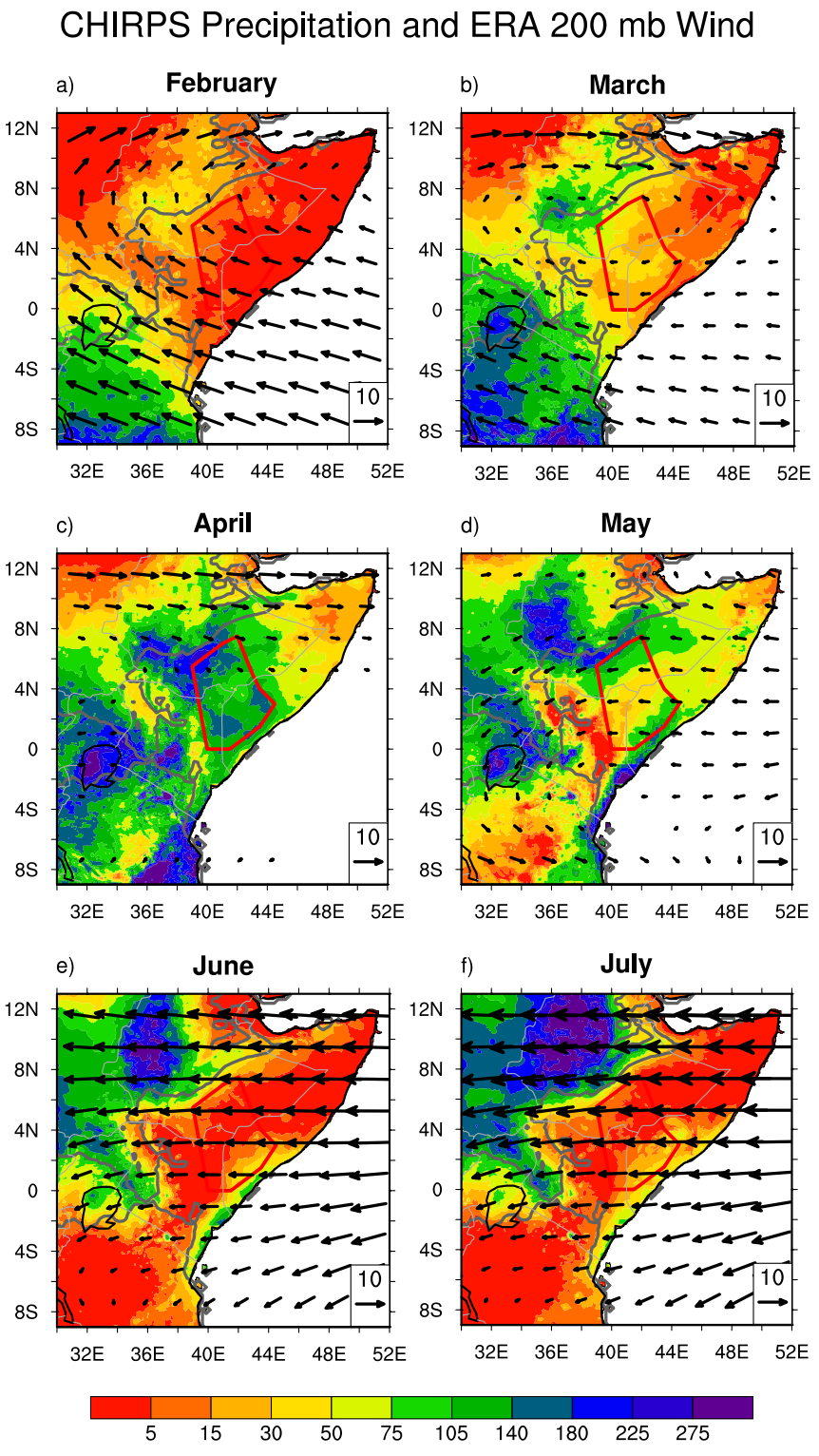

FIG. 3. Average monthly total precipitation (mm) estimated from CHIRPS (note uneven contour intervals) and 200-mb winds ($m\,s^{-1}$; reference vector in lower right of each map). Wind vectors are plotted every third grid point in latitude and longitude. Vectors are omitted at grid points with speeds less than $1\,m\,s^{-1}$. Polygon over eastern Horn of Africa indicates region over which data are averaged in subsequent analysis.

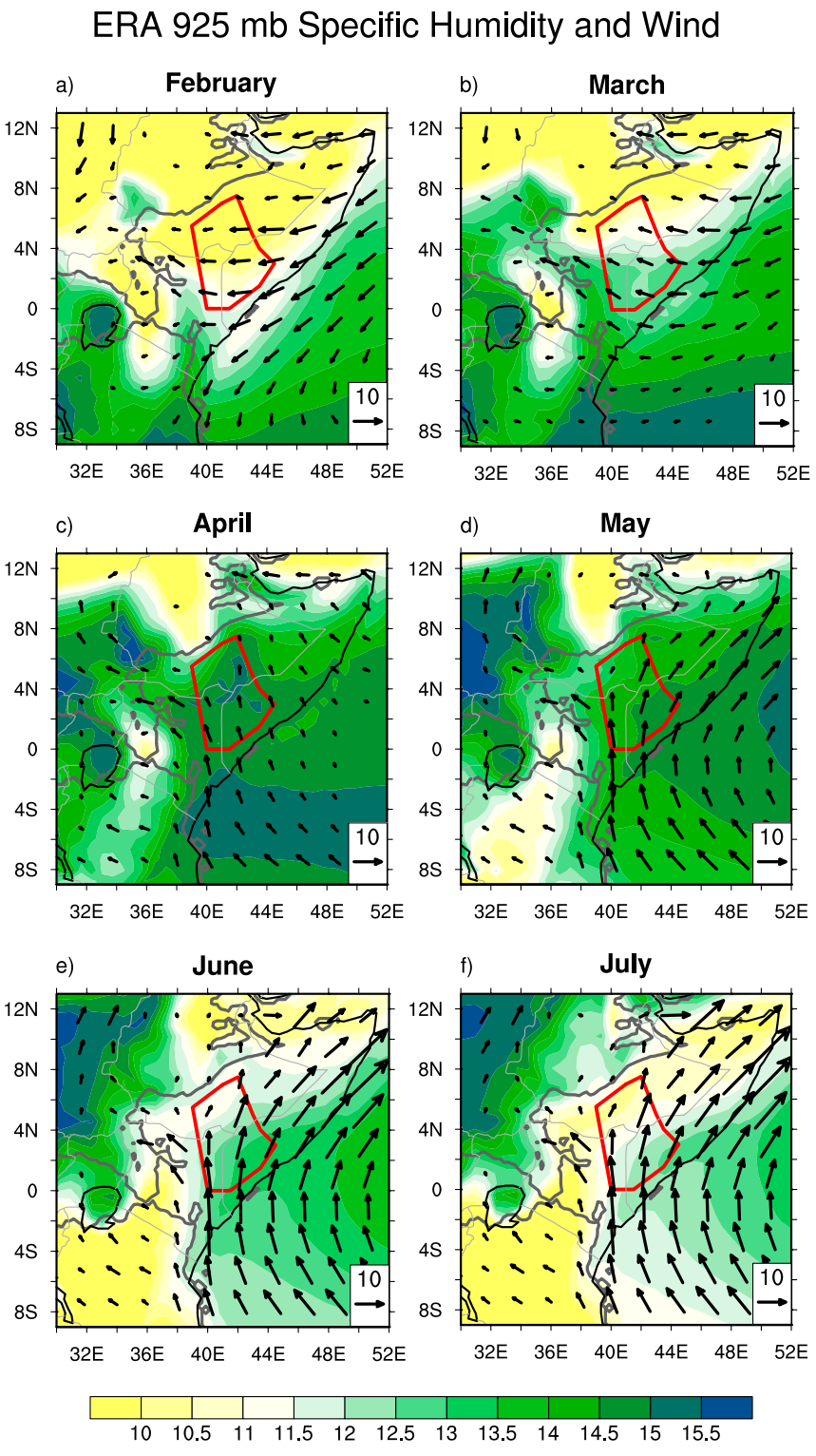

FIG. 4. As in Fig. 3, except specific humidity (g kg^{-1}) is shaded and vectors represent the 925-mb winds.

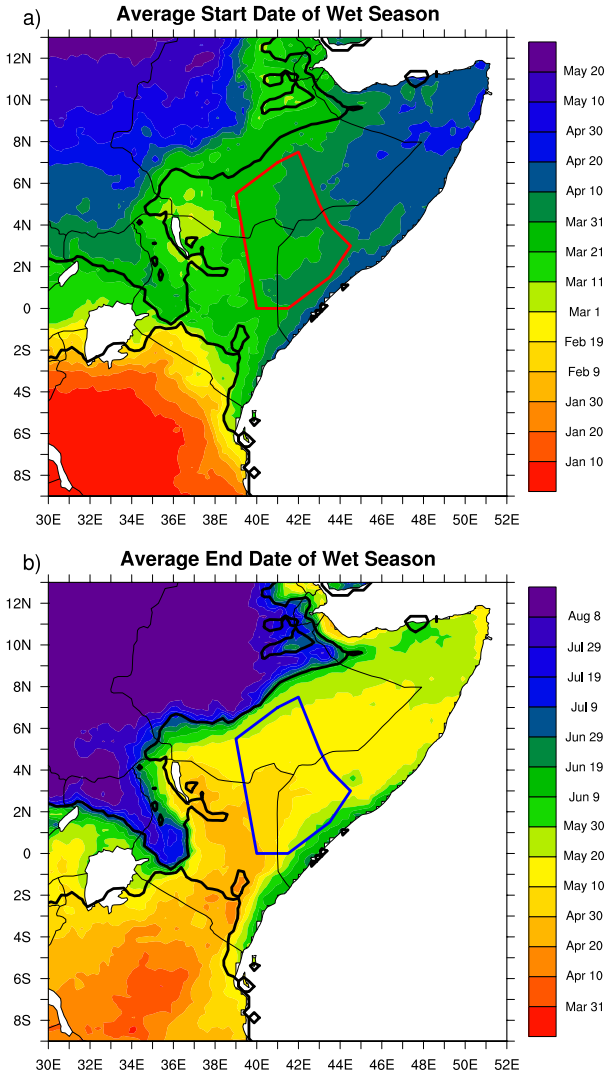

FIG. 5. (a) Average date of MAM wet season onset found by limiting search for onset to first half of calendar year. (b) Average last day of wet season. Red and blue polygons indicate region for subsequent detailed analysis. Black outline indicates region within which the ratio of the second to first annual harmonic is larger than 1 (which includes the area of the polygon and a small equatorial region to the west roughly between 2°S and 2°N).

Y15. As noted by Y15, these winds are also relatively dry because the coldest sea surface temperatures (SSTs) reside to the north of the equator at this time. In March (Fig. 4b), the near-coastal winds are weaker but have rotated clockwise and now have a substantial onshore component, resulting in a larger net moisture transport onto land, which is reflected in a specific humidity increase over the southern Horn. The peak of the wet season, April (Fig. 3c), is consistent with humidity values over land as high as those over the proximate ocean and with weak southerly winds advecting even higher humidity from the south-equatorial ocean (Fig. 4c). The southerlies continue to strengthen in May, June, and July, while specific humidity decreases (Figs. 4d–f), consistent with a cooling of the ocean, as discussed by Y15. These authors identify these strong southerly winds as the eastern Africa low-level jet (Findlater 1969), which is part of the Asian monsoon system and commences with the onset of the Indian monsoon (e.g., Halpern and Woiceshyn 2001). They also noted that those low-level winds are divergent over the eastern Horn at this time, consistent with the suppression of precipitation.

The low-level climatology, as examined in Y15, emphasizes the importance of low-level moisture advection for the annual cycle of precipitation in the eastern Horn of Africa: the seasonal variations in moisture supply and rainfall are related to those of the upwind coastal SSTs, which are coldest during the dry seasons. As we have shown in Fig. 3, however, the upper-level climatological winds also reveal an apparent relationship between the upper circulation over the western Indian Ocean/Horn region and Horn precipitation during the first half of the year, with strong easterlies systematically coinciding with low rainfall and no easterlies observed at the peak of the spring wet season. The monthly mean maps thus suggest that weak (strong) upper-level easterlies over the eastern Horn act to favor (inhibit) convection there, with both the upper- and lower-level winds being linked to the Asian monsoon system.

b. *Onset and demise of the long rains*

The average long rains onset and end dates at each grid point are shown in Fig. 5, with the methodology for this calculation explained in section 2. The region south of 2°S (Tanzania) should be disregarded as it is located mostly in the single-wet-season regime (Fig. 1b) and onset there occurs much earlier than 1 January, when the sun moves south during austral spring (saturated red colors in Fig. 5a). Over the eastern Horn, the wet season generally progresses northward from early March to the end of April. Onset occurs earlier over the western Horn than to the east and even earlier just east of the mountains (which generally follow the black harmonic ratio contour north of the equator). To the west of the mountains, onset occurs later, the timing consistent with a summertime rainfall maximum.

The end of the wet season also progresses northward over the bimodal region, varying from mid-April in the south to near the end of May in the north. These dates are consistent with a dry June there (Fig. 3e). To the west, the end occurs substantially later, in line with a single wet season, peaking in summer.

To better document the onset of the wet season at the daily time scale, daily composites of precipitation and other variables are constructed. For this analysis, a

target region was chosen for which the climatological wet season starting and end dates were relatively spatially homogeneous; in this polygonal region (outlined with a red contour in Fig. 5), the average onset date is 27 March. Figure 6 shows composites of precipitation and 200-mb winds relative to this mean onset date, shown every 4 days from 20 days prior to onset up to onset. While the chosen region was slightly modified during experimentation, the associated field patterns are generally robust. Prior to onset, precipitation is confined mainly to the sector in the Southern Hemisphere that is dominated by a single annual harmonic, as well as some small areas at the equator and in the mountainous regions of Ethiopia. Precipitation increases dramatically north of the equator on the day of onset (Fig. 6f), especially to the west of the target region (but still within the bimodal rainfall region, delineated by the gray contour), while the northern Horn is still dry. Strong upper-level easterly winds near the southern coast on day −20 (Fig. 6a) veer and become weak southeasterlies by day −8 (Fig. 6d). The weak anticyclone centered around 8°N, 36°E on day −20 (Fig. 6a) gradually expands eastward and becomes a clockwise circulation that straddles the equator and is most developed at day −4 (Fig. 6e). By onset (Fig. 6f), this clockwise circulation extends over the entire eastern Horn, with little upper-level flow over the target area.

Corresponding composites of 925-mb specific humidity and wind are displayed in Fig. 7. The offshore low-level winds, which are slightly northeasterly at day −20 (Fig. 7a), progressively develop a southerly component such that by onset (Fig. 7f) they appear to be advecting the relatively moist maritime air that lies to the south into the eastern Horn. This is entirely in agreement with the climatologies presented by Y15, who show that the off-coastal 10-m winds shift from northeasterly during January–February to southeasterly during MAM and note that, in the Southern Hemisphere equatorial region from which these winds flow, climatological SSTs are at their annual peak. The gradual increase in low-level moisture is also qualitatively consistent with an increase in CAPE (not shown) and in keeping with Y15, who found the low-level moist static energy to be maximum in MAM and dominated by the moisture term.

The same fields are now composited about the end of the wet season, whose climatological last day within the polygon is 18 May. The 200-mb winds remain weak over the Horn from day −19 to day −11 (Figs. 8a–c), while moderate westerlies are observed north of 8°N and south of 4°S. The easterly winds pick up over the Horn and western Indian Ocean on day −7 (Fig. 8d) and continue to strengthen throughout the sequence. At the same time the westerlies to the north and south disappear. We speculate that the sudden increase in upper-level easterlies is associated with the onset of the Asian and Indian monsoons, which occurs climatologically between May and June, as is evident when comparing Figs. 2d and 2e. Precipitation over the Horn, although variable from lag to lag, persists until the first day of the dry season (Fig. 8f), when it ceases abruptly.

Figure 9 shows 925-mb wind and specific humidity, composited relative to the last day of the wet season. The 925-mb winds over the eastern Horn remain southerly and steadily increase throughout the sequence. Again, these composites are consistent with the 10-m wind seasonal averages computed by Y15, which show the eastern Africa low-level jet (Findlater 1969), already evident during MAM, strengthening into northern summer. Like the upper-level easterlies that develop over the Horn and western Indian Ocean, these winds are components of the Asian monsoon (e.g., Y15). Contrary to the situation during onset (Fig. 7), the low-level moisture is maximum at the equator, and so the southerlies are now advecting comparatively dry air into the Horn from the south. This change is in agreement with a decrease in CAPE observed in the corresponding composites (not shown); it is also qualitatively consistent with the decrease in the moisture component of moist static energy and the increase in stability from northern spring to summer reported by Y15.

To better illustrate our findings, Fig. 10 shows detailed onset and end composites of the quantities shown in Figs. 6–9, as well as CAPE, but averaged over the polygonal target area. For reference, the 34-yr daily climatology is also shown (blue line); the first and last days of the composite wet season (day 0) are aligned with the climatological onset and end dates in the respective plot, to allow for comparison with the climatological cycle. No smoothing is applied to the time series. There is a clear precipitation signal for both onset and end, with a rapid jump at onset (Fig. 10a) and an equally precipitous decline at the end (Fig. 10e), despite the fact that both the composites and climatology are noisy during the wet season.

Corresponding composites for upper-level zonal wind are shown in Figs. 10b,f. The upper-level easterlies weaken rather suddenly about two weeks prior to onset, becoming weakly westerly or near zero around onset (Fig. 10b). They remain so for the rest of the composite (except for a brief excursion to easterly around day +6), while climatological easterly winds more gradually decrease to their postonset near-zero (or westerly) mean value. We note that using an expanded domain for the wind average yields quite similar results (not shown).

At the end of the wet season (Fig. 10f) there is a reverse rapid change from weak westerlies to strong

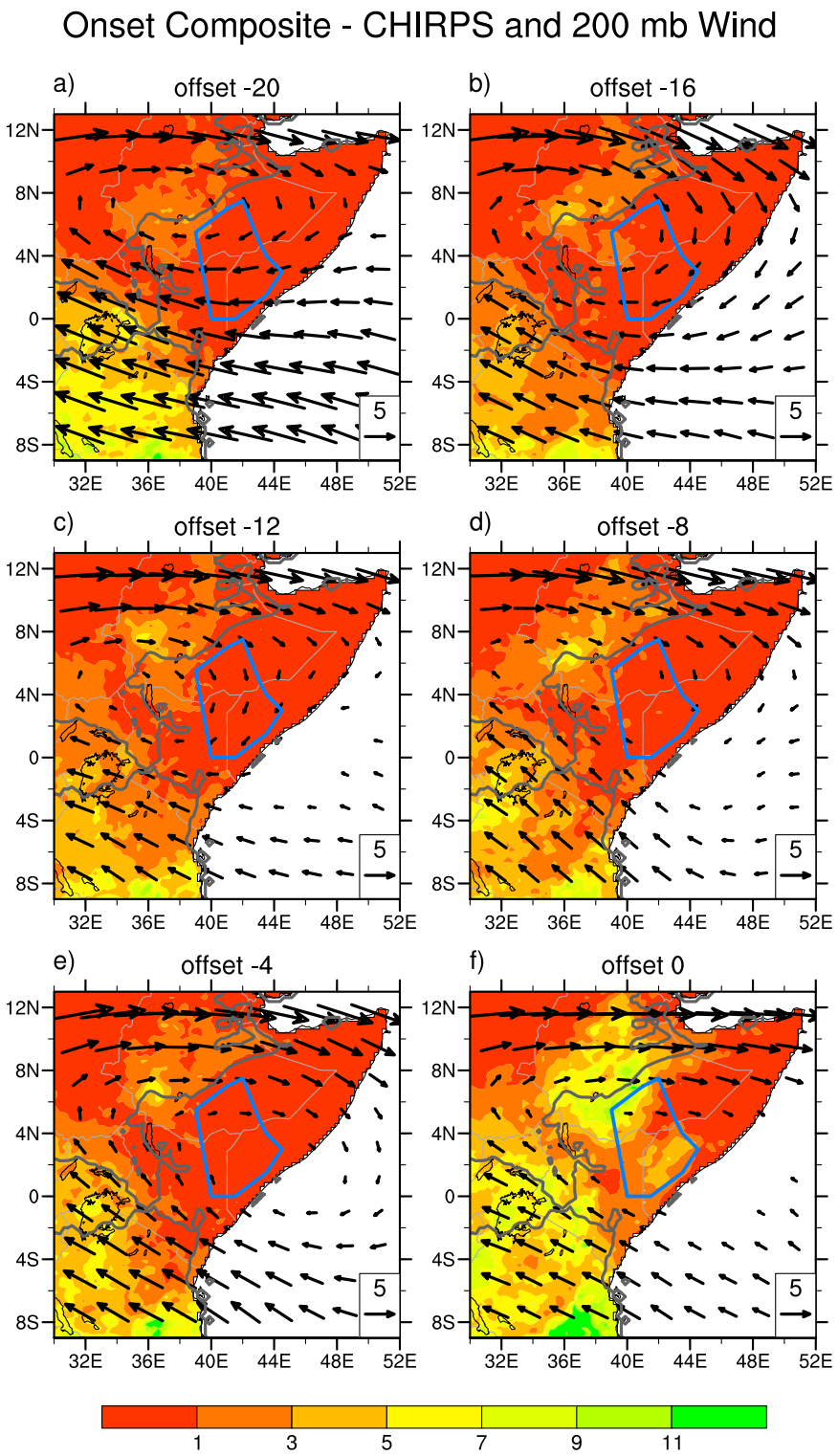

FIG. 6. Composite relative to interannually varying onset day (day 0) of precipitation (shaded; mm day^{-1}) and 200-mb winds (reference vector in lower right of plot is 5 m s^{-1}). Vectors are omitted if wind speed is less than 1 m s^{-1}. Dark gray contour indicates that the ratio of the second to first annual harmonic is equal to 1.

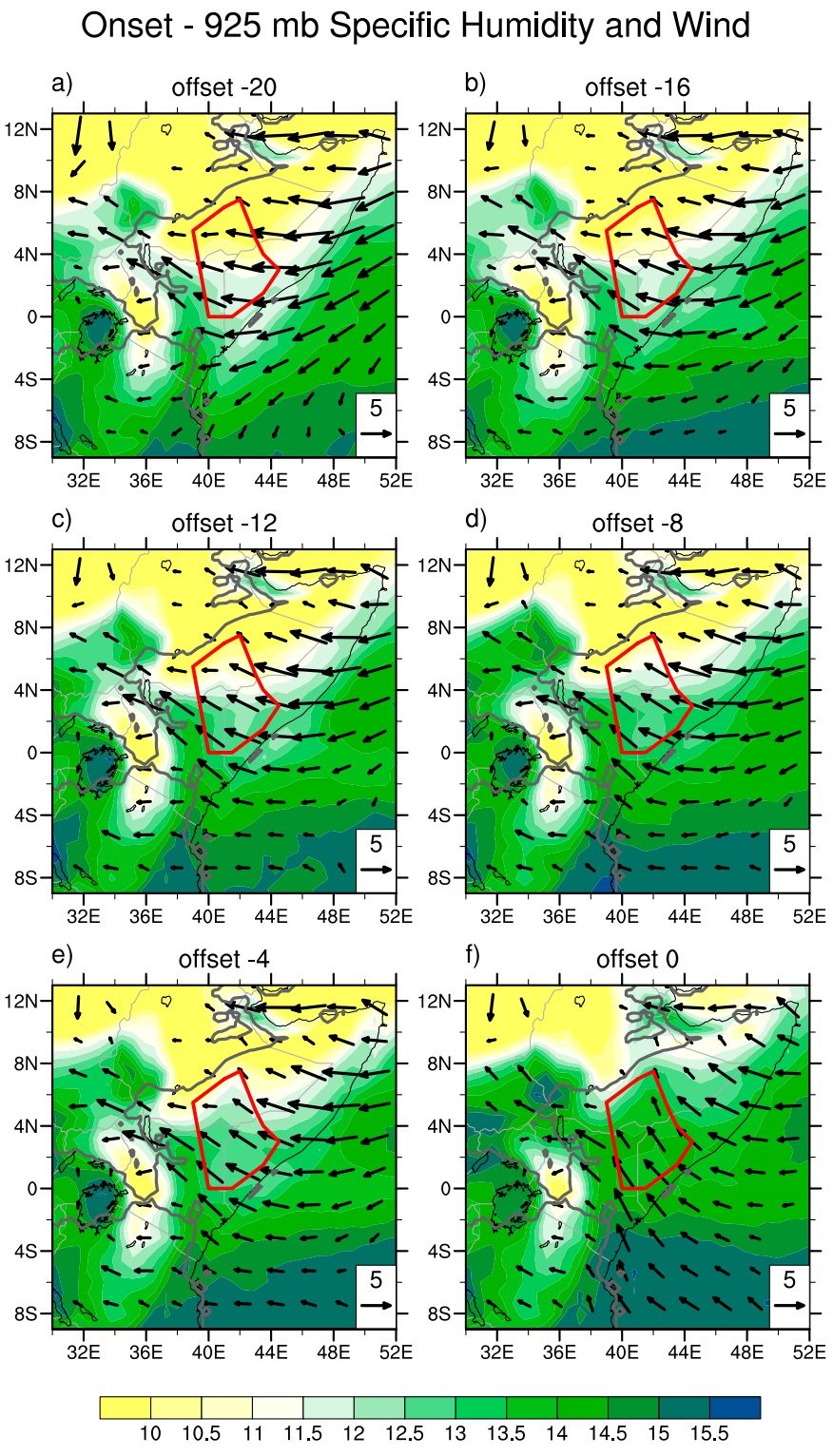

FIG. 7. Composite relative to interannually varying onset of specific humidity (shaded; g kg^{-1}) and 925-mb winds (reference vector in lower right of plot is 5 m s^{-1}).

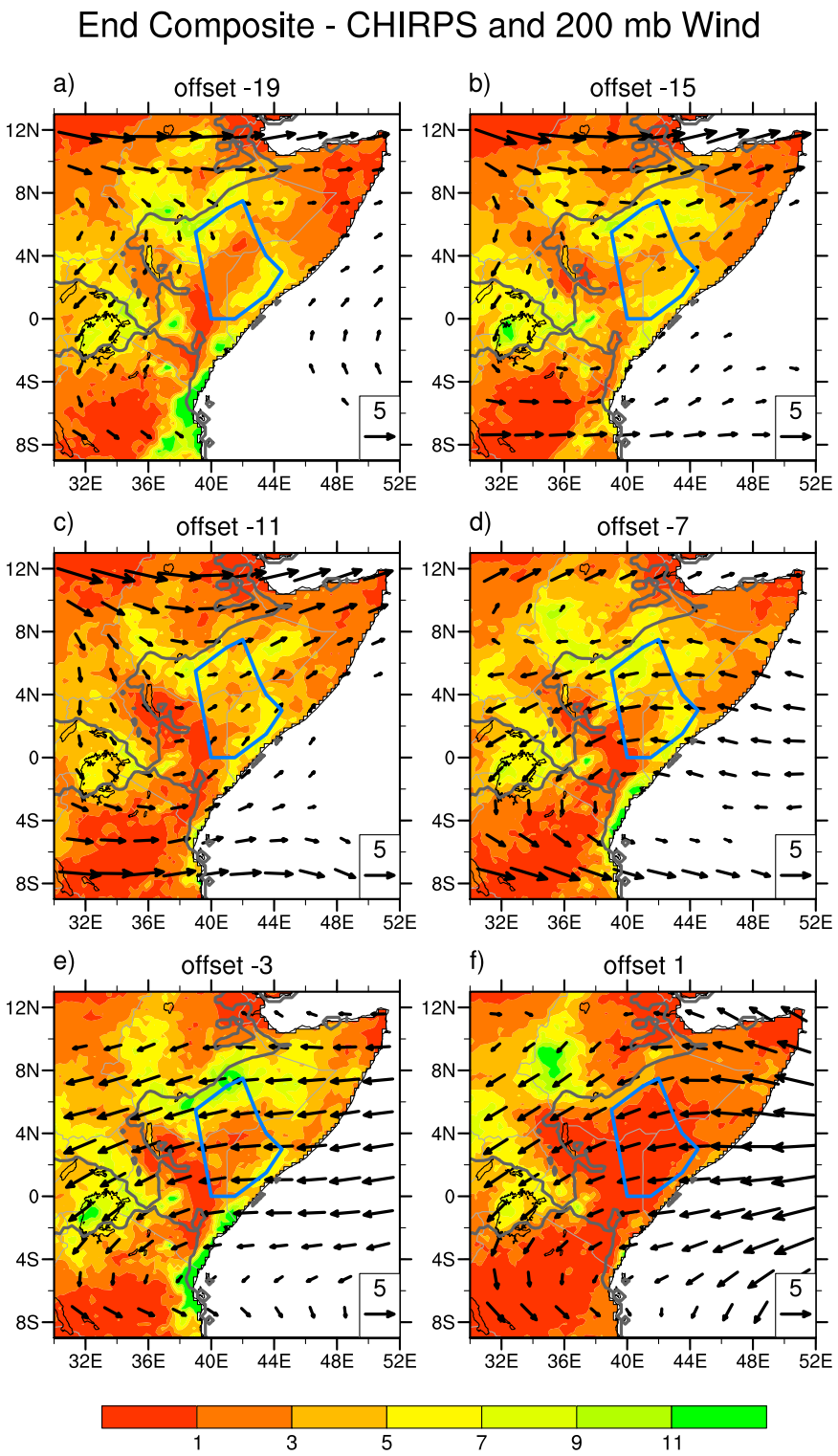

FIG. 8. As in Fig. 6, except relative to last day of wet season.

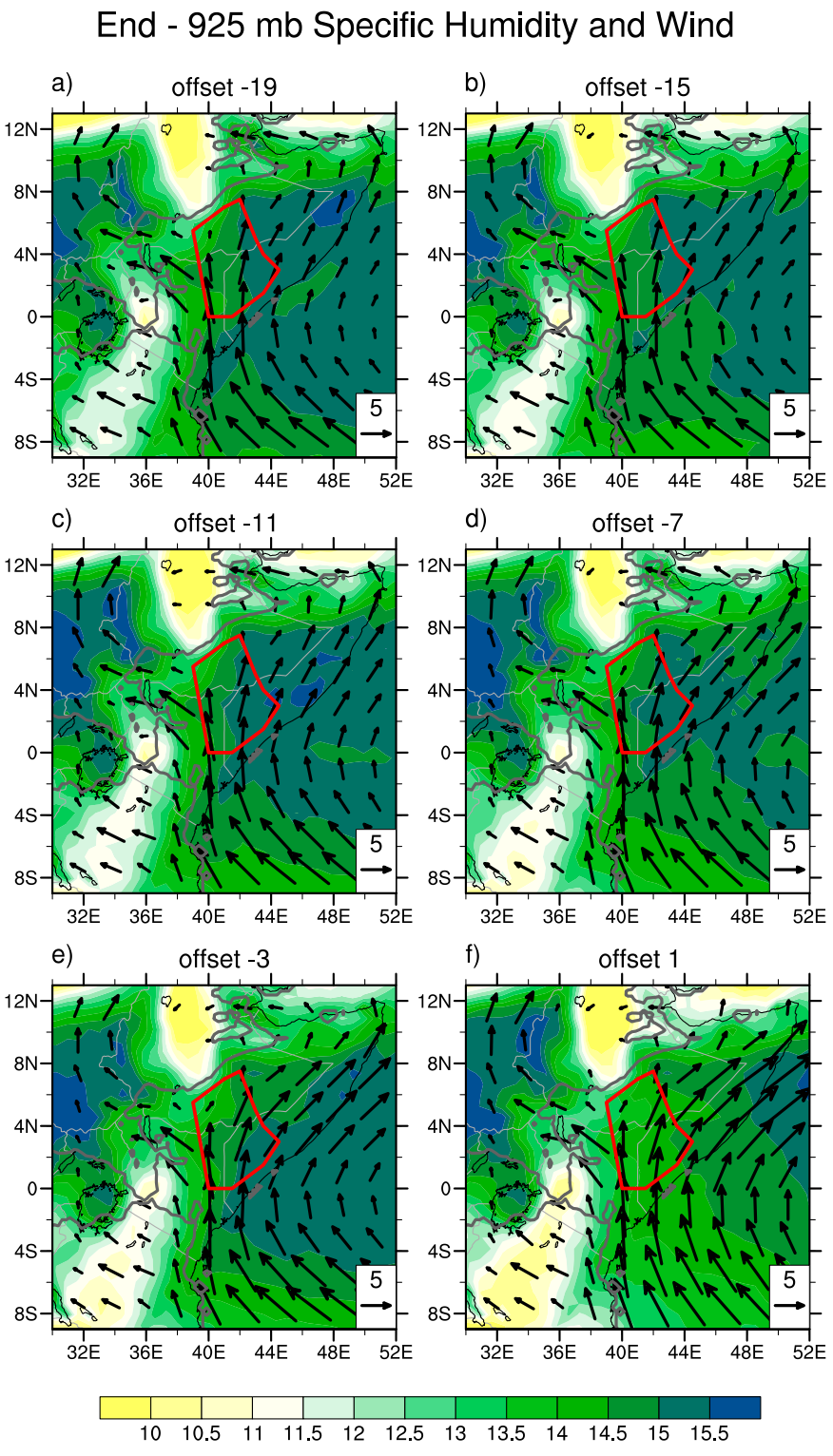

FIG. 9. As in Fig. 7, except relative to last day of wet season.

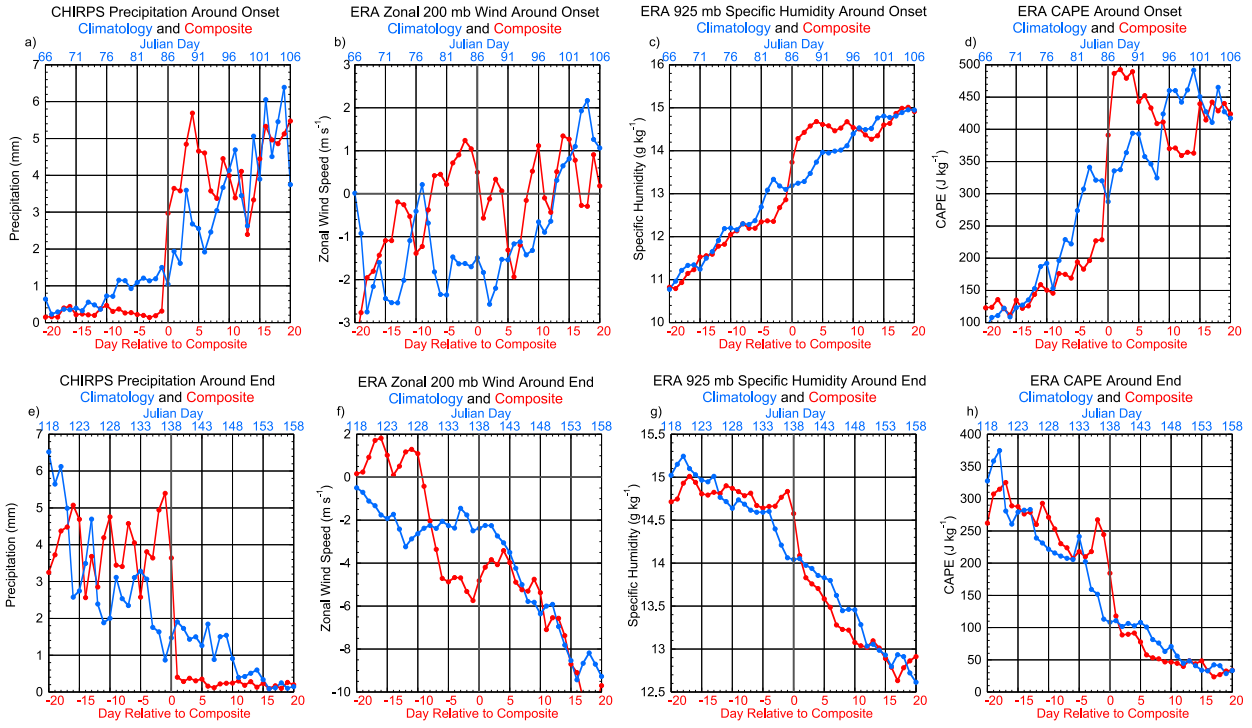

FIG. 10. Composite (red curves) and climatology (blue curves) of precipitation, 200-mb winds, 925-mb specific humidity, and CAPE averaged over the polygon shown in previous figures. (a)–(d) Composites are relative to onset, with day 0 set at Julian day 86, which is the average onset date (27 March). (e)–(h) The corresponding composites relative to the average last day of the wet season, Julian day 138, corresponding to 18 May.

easterlies that appears to occur in two steps: the winds start reversing around 10 days before the season's end, remain steady and moderately easterly for several days around the end, and then intensify further. The climatology about the average end date (18 May) is also characterized by a rapid two-step switch on of easterly winds, separated by a period of little change. After the flat stage, easterlies increase in both the composite and climatological sequences at an equal rate. We speculate that the returning upper-level easterlies suppress precipitation either directly, through enhanced upper-level convergence and subsidence, or indirectly, by preventing extratropical disturbances from penetrating into the Horn region and triggering vertical motion (we will return to this later).

Last, the composites and climatologies of 925-mb specific humidity and CAPE are presented in the two rightmost columns. The climatological onset occurs during a prolonged period of slowly increasing specific humidity (Fig. 10c) and CAPE (Fig. 10d). In contrast, the composites show rapid increases in these variables right around onset, leveling off thereafter while the climatology "catches up." The corresponding composite and climatology curves about the rain season last day (Figs. 10g,h) are more similar to each other, but the evolution is still sharper in the composites, with rapid decreases in both humidity and CAPE around the last wet day.

Our view of onset and end, based on Fig. 10, is that the actual dates of onset and end of the wet season in a particular year constitute a slight departure in timing from the average annual cycle. The precipitation composite, when compared to climatology, provides the most obvious example of this shift, but the same is true of the zonal wind, specific humidity, and CAPE evolution. There is almost no precipitation before onset or after the end, with large jumps occurring on the onset and end dates. Likewise, the composite winds are more westerly at onset relative to climatology and more strongly easterly at the end. The composite evolutions of 925-mb specific humidity and CAPE also are of the expected sign: moister and with more CAPE than climatology at onset and drier and with less CAPE than climatology at the end.

c. *Changes in seasonal totals since 1981*

The ultimate motivation for this study was to determine the extent to which changes in the various long-rain characteristics have contributed to the observed decrease since the early 1980s (e.g., Funk et al. 2008;

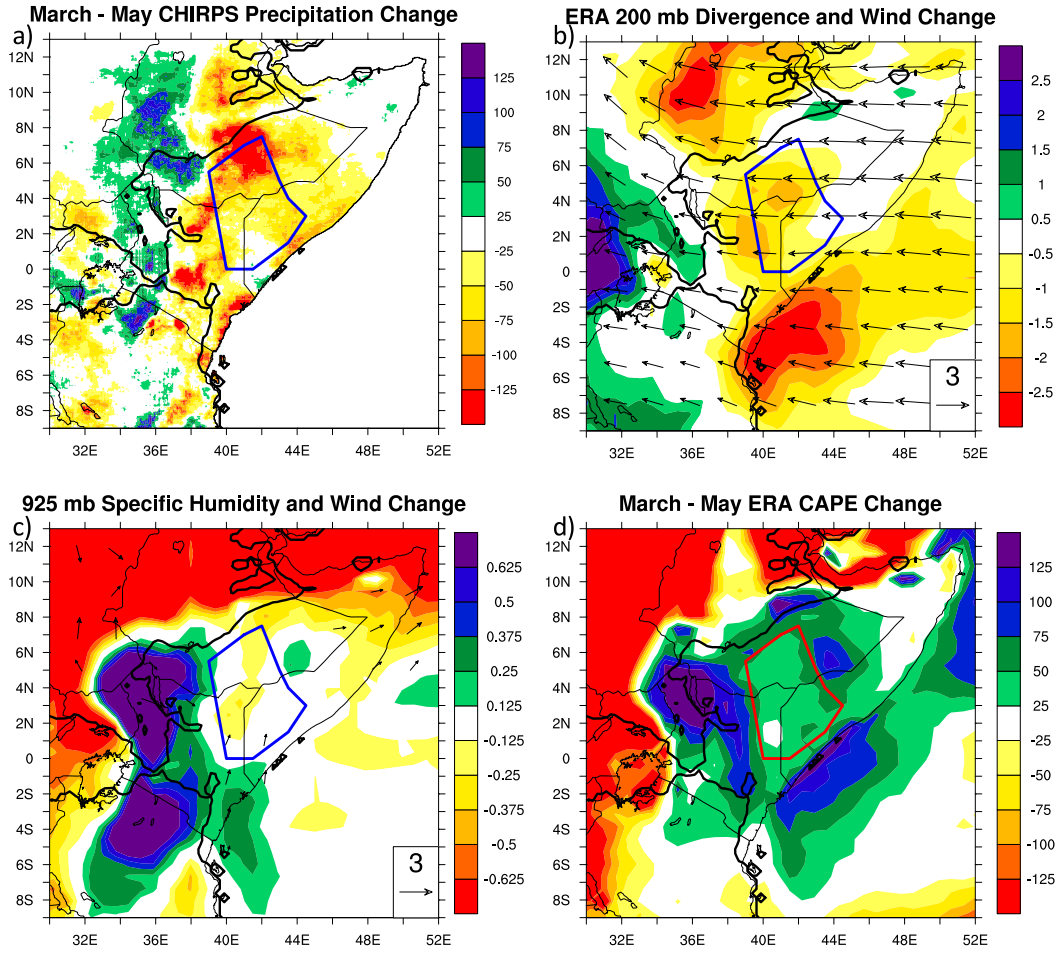

FIG. 11. The 1981–2014 change (defined as least squares fit linear trend multiplied by 33 yr) of MAM (a) CHIRPS precipitation (mm), (b) 200-mb divergence (s^{-1}; scaled by 10^{-6}) and wind, (c) 925-mb specific humidity ($g\,kg^{-1}$) and wind, and (d) CAPE ($kg\,s^{-1}$). In (b) and (c), reference wind vector is shown in lower right ($m\,s^{-1}$). Vectors are plotted at alternating grid points. Vectors less than $1\,m\,s^{-1}$ are not plotted. Polygons represent area of detailed study. On all maps, black contour indicates a ratio between the second and first annual harmonic equal to 1. The polygon is within the area of ratio greater than 1.

Williams and Funk 2011; Lyon and DeWitt 2012; Liebmann et al. 2014) and to assess whether the recent tendency for failed long rains can be understood as a weakened or an altered seasonal cycle. This decrease in the March–May wet season from 1981 to 2014, expressed as a change (linear least squares fit trend multiplied by 33 yr) and estimated from CHIRPS data, is shown in Fig. 11a. The decline over the eastern Horn is widespread, with the largest decreases in southern Ethiopia, in the northern end of the polygon. Weaker increases are evident to the west, in the single-wet-season regime over western Ethiopia and central/southern Tanzania, but March–May is not the peak of the wet season there. The change in MAM CHIRPS precipitation averaged over the Horn polygon is −64.8 mm, or a decrease of 28% relative to the mean (232 mm). A huge positive anomaly occurred in 1981, the largest seasonal total on record, with many more rainy days than normal, and if that year is excluded the linear decrease halves to −32.0 mm, but in other respects (season length and daily rain rate) that year is not an outlier, so the year will be included in subsequent analyses.

We now examine how the precipitation intraseasonal characteristics that determine the seasonal totals have changed since 1981. For the period 1981–2014, the average wet season total within the polygonal area is 216 mm (ranging from 99 to 434 mm) and the average season length is 53 days (ranging from 27 to 89 days), beginning on average on 27 March (with a range from 26 February to 24 April) and ending on 18 May (with a range from 1 May to 2 June). The average daily rain rate (the wet season total divided by its length) is thus

4.1 mm day^{-1} (varying between 2.2 and 6.8 mm day^{-1}). The wet season rain rate decreased over the record period by 0.88 mm day^{-1}, so if the average wet season length had remained constant at 53 days, the drop in precipitation accounted for by the reduced rate would have been 46.6 mm. The length, however, also decreased by 3.2 days (~6%), so if the rain rate had remained constant the shortening of the season would have accounted for a 13.1-mm reduction. The wet season contraction has resulted mainly from a delay of 4.2 days in the starting date, partly compensated for by a 1-day delay in end date. The above result thus implies that the most important contributor to the observed decline of MAM precipitation in the central Horn of Africa since 1981 is the reduction in the within-season precipitation (or rain rate) rather than a shortened length, at least in our target area. In contrast, Camberlin et al. (2009) found that in the southern Horn, variations in onset date have the most influence on interannual variations of seasonal totals.

To explore possible thermodynamical and dynamical causes of this decline, Figs. 11b–d display the corresponding changes in 200-mb winds and divergence, 925-mb winds and humidity, and CAPE over the Horn region. While advection of low-level moisture is a crucial ingredient of wet season precipitation, as shown earlier and also in Y15, the analysis reveals little change in specific humidity over the 34-yr record (note the small contour interval) and the same for the low-level wind field. Likewise CAPE does not appear to have decreased at all. Thus, the long-term decline in long-rain precipitation cannot be accounted for by a decrease in low-level moisture or potential instability. On the other hand, the upper-level circulation exhibits some remarkable changes, with a broad-scale shift toward stronger easterlies, about 3 m s^{-1} in magnitude. The change is smaller to the west, implying a tendency for upper-level net zonal inflow into the Horn region. Indeed, over most of the domain (including over the northwest, where precipitation has increased) ERA-Interim data indicates an increase in convergence, suggesting enhanced downward motion. The strengthening of the 200-mb easterlies that has accompanied the drying trend in the long rains is consistent with our earlier intraseasonal analysis that shows that precipitation in MAM tends to occur when the easterlies falter and to stop when they resume.

Moreover, the above signal is part of a widespread increase in easterlies that extends to most of eastern Africa and the Indian Ocean, as shown in Fig. 12a, which also displays the corresponding 1981–2014 large-scale change in precipitation, with OLR as a proxy for rainfall. The increase in precipitation over Indonesia is likely due to enhanced warming of the Indian Ocean and western Pacific (e.g., Hartmann et al. 2013) and has been hypothesized (but not shown) to have enhanced the Indian Ocean Walker circulation (e.g., Williams and Funk 2011), thereby increasing subsidence and decreasing precipitation over the Horn. To validate this hypothesis, Fig. 12b presents a cross section of the change in divergence, zonal wind, and omega velocity, meridionally averaged within the box depicted in Fig. 12a. Clearly the picture is not a simple one of an enhanced closed zonal cell extending from Indonesia to the Horn. There is increased upward motion and upper-level divergence over Indonesia (consistent with the decrease in OLR; Fig. 12a), upper-level easterly outflow over the entire Indian Ocean between 250 and 125 hPa, and upper-level convergence in the western end of the transect, including over the Horn region, as already mentioned (Fig. 11b). The accompanying subsidence, however, is limited to the western Indian Ocean and does not extend to the Horn region, where upward motion is seen instead, and even over the ocean there is no clear signal of compensating lower-level divergence. Moreover, although a closed zonal anomalous circulation is evident, it is confined to the western Indian Ocean, with upward motion near 75°E.

Although the ERA-Interim circulation changes appear to be inconsistent with the observed MAM decrease in precipitation and increase in OLR (Figs. 11a and 12a) over the eastern Horn, they are consistent with an increase in ERA-Interim precipitation there (Fig. 12c). This discrepancy between ERA-Interim and observed precipitation calls into question the validity of the ERA-Interim divergent circulation over the Horn of Africa region.

4. Summary and discussion

The eastern Horn of Africa has an interesting and unusual climate in that the double-wet-season regime that is present at most longitudes around the equator—an example of which can be found just to the west of the Horn (Fig. 1b)—extends well north of the equator. Moreover, the annual cycle's timing is such that the eastern Horn is dry when the rest of Africa at the same latitude is experiencing its climatological rainfall maximum (i.e., boreal summer). This study has attempted to clarify the dynamics and thermodynamics of the climatological ''long rains'' (March–May), with the aim of making progress into understanding their recent observed decline.

An examination of monthly climatologies of precipitation and 200-mb wind reveals that strong upper-level easterlies coincide with low precipitation—a finding that, to our knowledge, has not been reported in other studies. In particular, there is a dramatic strengthening of easterlies that accompanies the shutdown of precipitation from May to June. These strong easterlies

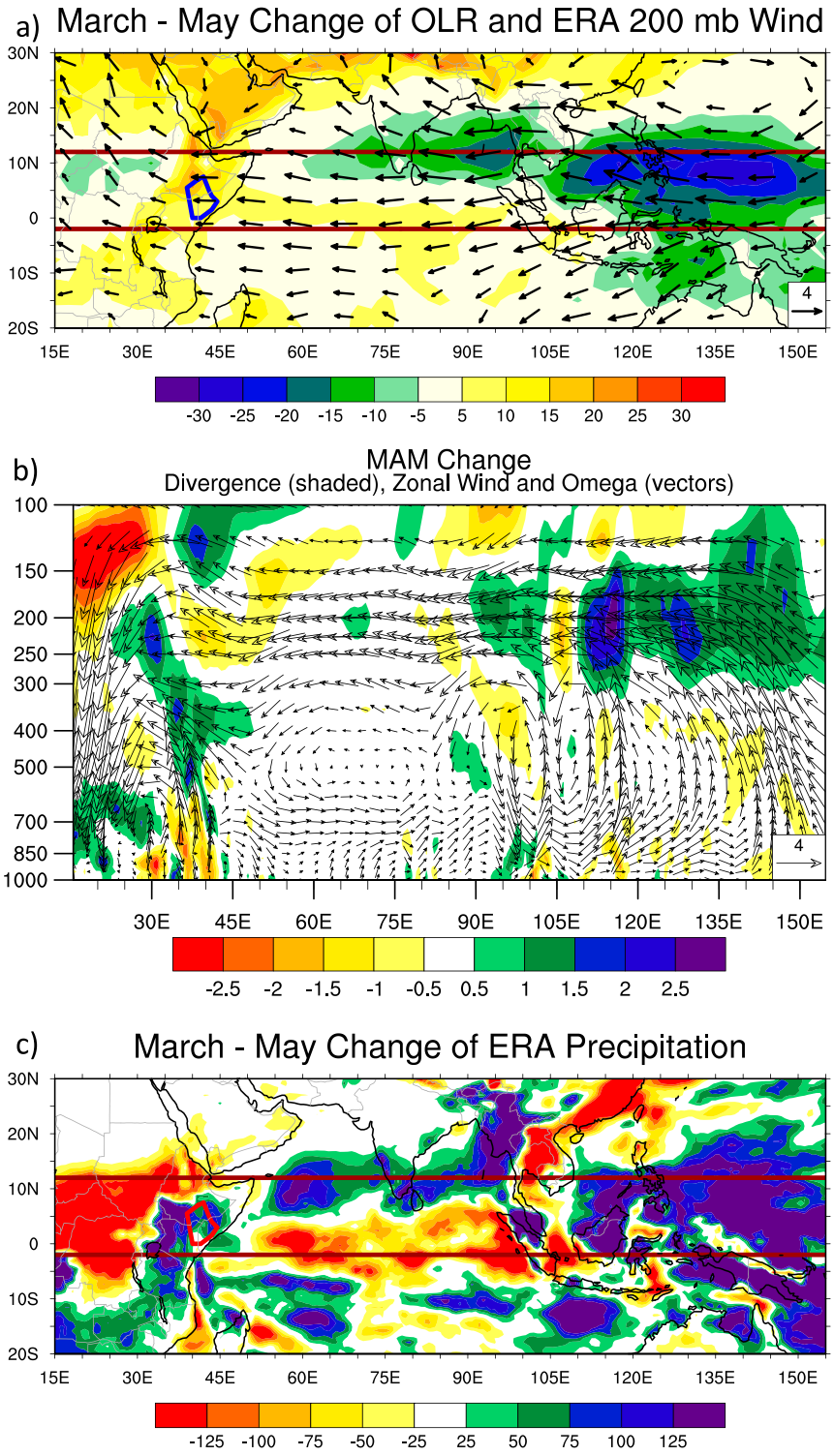

FIG. 12. (a) Change in MAM OLR (shading) and 200-mb wind (vectors; m s^{-1}; reference in lower right corner; plotted at every 6th grid point in latitude and 12th grid point in longitude) for 1981–2014. (b) Cross section of the change in divergence (shaded; s^{-1}; multiplied by 10^6) and zonal wind and omega (vertical) velocity (vectors). Quantities are averaged within latitudes 2°S–12°N indicated by dark red lines in (a). Vectors with magnitude greater than 1 m s^{-1} are plotted at every fourth grid point in the horizontal and at selected levels. Sign of the omega velocity is inverted, and value was converted such that the quantity shown is in millibar per 6 h. (c) Change in ERA-Interim precipitation for same period. Shading is as in Fig. 11a.

appear to be associated with the large-scale anticyclone that develops concomitantly with the onset of the Asian monsoon and are consistent with the response to an off-equatorial heat source (Gill 1980). Y15 showed that the dry seasons in the Horn coincide with low moist static energy, which they found to be dominated by the surface humidity term, but our results suggest that changes in the upper-level zonal winds also play a role in determining the start and end of the long rains.

Area-averaged composites of 200- and 925-mb winds, precipitation, specific humidity, and CAPE relative to the start and end of the long rains were computed for a relatively homogeneous region (in terms of start and end dates) within the eastern Horn (the polygon shown in all maps), in order to gain more insights into the precursor mechanisms. Precipitation exhibits a rapid increase at onset and a marked drop at the end, similar to, but more rapid than, the evolution of the annual cycle near the average onset and end dates, respectively (Figs. 10a,10e). Consistent with this, the changes in the 200-mb easterlies are also much more evident in the composites than in the climatology, with the decrease beginning several days before onset and with the increase at the end occurring much faster than in the climatology (Figs. 10b,10f). This result supports our contention that precipitation tends to occur when the upper-level easterlies dwindle or reverse to westerlies.

At low levels, our composites are consistent with those of Y15 (although they used different variables), in that there is a sharp increase and decrease in 925-mb specific humidity that precedes onset and end, respectively. As with the other quantities, the composite increase is superimposed upon a climatology that is also rapidly changing (Figs. 10c,10g). The composites again suggest that the individual years' wet season onset and end are deviations from the annual cycle (e.g., on average, an early onset occurs with weaker upper-level easterlies and higher low-level specific humidity than expected from climatology on that day). The original focus of this study was to try to identify a synoptic "trigger" associated with wet season onset, but we found no obvious signal. Our present view is that onset and end are determined locally when either favorable or unfavorable upper-level winds and low-level thermodynamic conditions have been established.

A summary of our argument as to the cause of the decline in long-rain precipitation since 1981 is the following. Low-level moisture and weak upper-level easterlies both occur concurrently with the long rains in monthly climatologies. The easterlies that prevail prior to the beginning of the wet season appear to be forced by diabatic heating originating in the Southern Hemisphere ITCZ in the central-to-eastern Indian Ocean. These easterlies slacken as the center of diabatic forcing shifts into the Northern Hemisphere and the eastern Horn long rains occur during this "break." The easterlies then resume when the Asian and Indian monsoon systems develop. In composites based on interannual onset (end), easterlies decrease (increase) several days prior to the sudden jump (drop) in precipitation. These easterly winds, which appear to be partly responsible for the annual shutdown of the boreal spring wet season, have increased in strength during MAM since 1981 as precipitation has decreased, which suggests that they are also involved in this observed decline of the long rains.

A main finding of this study is thus that an inverse relationship between the strength of the upper-level easterlies and Horn precipitation is evident on three time scales: climatological, intraseasonal, and multidecadal (on interannual time scales there is also a significant anticorrelation between Horn precipitation and easterlies aloft; not shown). On the other hand, low-level moisture, shown to be an important component of the long rains in Y15 and also herein, shows little change over the record and thus appears less likely to have played a role in the long-rain decline.

Based on our previous work and that of others (e.g., Williams and Funk 2011; Lyon and DeWitt 2012; Lyon 2014; Lyon et al. 2014), we further argue that the strengthening of the upper-level easterlies over the Indian Ocean in MAM has been driven by the increase in precipitation over Indonesia, shown in Fig. 12 with OLR as a proxy for rainfall. This increased convection has enhanced divergence aloft leading to intensified upper-level easterly outflow over the Indian Ocean. We speculate, but are unable to demonstrate at this point, that the increased upper-level easterly winds suppress Horn precipitation either directly, via increased downward motion, or indirectly. Although the divergence and omega fields in ERA-Interim data are not conclusive in this regard, there is time-mean subsidence in MAM over the eastern Horn (Y15), consistent with the notion that stronger converging easterlies aloft would act to increase subsidence in that region. The lack of agreement between observed and ERA-Interim precipitation trends since 1981 in the Horn region does not give us much confidence in the reliability of the ERA-Interim divergent circulation and prevents us from either validating or refuting our hypothesis.

It is also possible that there is a less direct connection between upper-level easterlies and precipitation. As these easterlies reverse to westerlies and the critical line vanishes, extratropical disturbances are able to propagate to the deep tropics (Webster and Holton 1982), a possibility that is consistent with the episodic nature of precipitation in the eastern Horn. A search for a "compositable" signal associated with equatorward-propagating disturbances, however, has not yet proved fruitful.

It is tempting to speculate that the increase in the *background* upper-level easterlies may be linked to the emerging teleconnection between west-central Pacific SSTs and eastern Africa rainfall documented in Liebmann et al. (2014). As the easterly outflow over the Indian Ocean from Indonesian convection has strengthened owing to the differential warming in the warm pool, the circulation may also have become more sensitive to changes in the western Pacific SST gradient and thus more effective at modulating eastern Africa rainfall, creating more opportunities for prediction (Funk et al. 2014).

It should also be mentioned that it is unclear whether the recent observed precipitation, SST, and circulation trends in the warm pool/Horn region are anthropogenically forced or are the result of natural multidecadal fluctuations unrelated to global warming. In particular, the linear precipitation trends in the Horn region are highly sensitive to choice of beginning and end year, to the presence of extremes, to the particular region under consideration, and the dataset used. For instance, for most of the Horn of Africa the downward trends are much weaker if computed from 1982 (as already mentioned for our polygon), while in many parts of the domain the trends computed for the last 15–25 yr are no longer negative because of one extremely rainy year toward the end of the record (2013; not shown). Additionally, updated trends are uncertain because of the delay in the incorporation of new station data into the gridded datasets. This makes it difficult to characterize the recent evolution of Horn precipitation as either a persistent downward trend (as suggested by Verdin et al. 2005; Williams and Funk 2011; Funk and Hoell 2015; Funk et al. 2015c), an abrupt decline around 1999 (as suggested by Lyons and Dewitt 2012), or multidecadal variability (as suggested by Lyon et al. 2014; Yang et al. 2014; Hoell et al. 2017). Nevertheless it is clear from examination of any time series that the region has exhibited a succession of very dry years since 1981.

Last, from a food security perspective, the reported 4-day delay in the start of the wet season since 1981 offers useful insight as it implies more frequent late season starts but with decent harvests still plausible (if seed is available to replant). For insecure households, there is a huge difference between no harvest (failed season, no possible replanting) and mediocre harvests (delayed onset). Effective rainfall monitoring and response strategies could help mitigate this change in precipitation distribution.

Acknowledgments. We thank all the reviewers for their excellent suggestions, leading to a much-improved manuscript. BL, DA, and XQ were funded by United States Agency for International Development, FEWSNET NA150AR4320137. IB was funded by COMETH CGL2012-30641 of the Spanish MICINN. CF was funded under the USGS Drivers of Drought project. PP was supported by U.S. Geological Survey (USGS) Cooperative Agreement (G09AC000001).

REFERENCES

AMS, 2012: Convective available potential energy. Glossary of Meteorology. [Available online at http://glossary.ametsoc.org/wiki/Convective_available_potential_energy.]

Camberlin, P., and N. Philippon, 2002: The East African March–May rainy season: Associated atmospheric dynamics and predictability over the 1968–97 period. *J. Climate*, **15**, 1002–1019, doi:10.1175/1520-0442(2002)015<1002:TEAMMR>2.0.CO;2.

——, and R. E. Okoola, 2003: The onset and cessation of the ''long rains'' in eastern Africa and their interannual variability. *Theor. Appl. Climatol.*, **75**, 43–54, doi:10.1007/s00704-002-0721-5.

——, V. Moron, R. Okoola, R. N. Philippon, and W. Gitau, 2009: Components of rainy seasons' variability in equatorial East Africa: Onset, cessation, rainfall frequency and intensity. *Theor. Appl. Climatol.*, **98**, 237–249, doi:10.1007/s00704-009-0113-1.

Dunning, C. M., E. C. L. Black, and R. P. Allan, 2016: The onset and cessation of seasonal rainfall over Africa. *J. Geophys. Res. Atmos.*, **121**, 11 405–11 424, doi:10.1002/2016JD025428.

ECMWF, 2009: ERA-Interim project. Research Data Archive at the National Center for Atmospheric Research, Computational and Information Systems Laboratory, accessed 6 February 2015, doi:10.5065/D6CR5RD9.

Findlater, J., 1969: A major low-level air current near the Indian Ocean during the northern summer. *Quart. J. Roy. Meteor. Soc.*, **95**, 362–380, doi:10.1002/qj.49709540409.

Funk, C., and A. Hoell, 2015: The leading mode of observed and CMIP5 ENSO-residual sea surface temperatures and associated changes in Indo-Pacific climate. *J. Climate*, **28**, 4309–4329, doi:10.1175/JCLI-D-14-00334.1.

——,G. Senay, A. Asfaw, J. Verdin, J. Rowland, J. Michaelsen, D. Korecha, and R. Choularton, 2005: Recent drought tendencies in Ethiopia and equatorial subtropical eastern Africa. U.S. Agency for International Development Rep., 12 pp. [Available online at pdf.usaid.gov/pdf_docs/PNADH997.pdf.]

Funk, C., M. D. Dettinger, J. C. Michaelsen, J. P. Verdin, M. E. Brown, M. Barlow, and A. Hoell, 2008: Warming of the Indian Ocean threatens eastern and southern African food security but could be mitigated by agricultural development. *Proc. Natl. Acad. Sci. USA*, **105**, 11 081–11 086, doi:10.1073/pnas.0708196105.

——, A. Hoell, S. Shukla, I. Bladé, B. Liebmann, J. B. Roberts, and G. Husak, 2014: Predicting East African spring droughts using Pacific and Indian Ocean sea surface temperature indices. *Hydrol. Earth Syst. Sci.*, **18**, 4965–4978, doi:10.5194/hess-18-4965-2014.

——, A. Verdin, J. Michaelsen, P. Peterson, D. Pedreros, and G. Husak, 2015a: A global satellite-assisted precipitation climatology. *Earth Syst. Sci. Data*, **7**, 275–287, doi:10.5194/essd-7-275-2015.

——, and Coauthors, 2015b: The climate hazards infrared precipitation with stations—A new environmental record for monitoring extremes. *Sci. Data*, **2**, 150066, doi:10.1038/sdata.2015.66.

——, S. E. Nicholson, M. Landsfeld, D. Klotter, P. Peterson, and L. Harrison, 2015c: The Centennial Trends Greater Horn of Africa precipitation dataset. *Sci. Data*, **2**, 150050, doi:10.1038/sdata.2015.50.

Gill, A. E., 1980: Some simple solutions of heat-induced tropical circulation. *Quart. J. Roy. Meteor. Soc.*, **106**, 447–462, doi:10.1002/qj.49710644905.

Halpern, D., and P. M. Woiceshyn, 2001: Somali jet in the Arabian Sea, El Niño, and India rainfall. *J. Climate*, **14**, 434–441, doi:10.1175/1520-0442(2001)014<0434:SJITAS>2.0.CO;2.

Hartmann, D. L., and Coauthors, 2013: Observations: Atmosphere and surface. *Climate Change 2013: The Physical Science Basis*, T. F. Stocker et al., Eds., Cambridge University Press, 159–254. [Available online https://www.ipcc.ch/pdf/assessment-report/ar5/wg1/WG1AR5_Chapter02_FINAL.pdf.]

Hastenrath, S., 2000: Zonal circulations over the equatorial Indian Ocean. *J. Climate*, **13**, 2746–2756, doi:10.1175/1520-0442(2000)013<2746:ZCOTEI>2.0.CO;2.

——, D. Polzin, and C. Mutai, 2007: Diagnosing the 2005 drought in equatorial East Africa. *J. Climate*, **20**, 4628–4637, doi:10.1175/JCLI4238.1.

——, ——, and ——, 2011: Circulation mechanisms of Kenya rainfall anomalies. *J. Climate*, **24**, 404–412, doi:10.1175/2010JCLI3599.1.

Hoell, A., and C. Funk, 2014: Indo-Pacific sea surface temperature influences on failed consecutive rainy seasons over eastern Africa. *Climate Dyn.*, **43**, 1645–1660, doi:10.1007/s00382-013-1991-6.

——, M. Hoerling, J. Eischeid, X.-W. Quan, and B. Liebmann, 2017: Reconciling theories for human and natural attribution of recent East Africa drying. *J. Climate*, **30**, 1939–1957, doi:10.1175/JCLI-D-16-0558.1.

Hutchinson, P., 1992: The Southern Oscillation and prediction of ''Der'' season rainfall in Somalia. *J. Climate*, **5**, 525–531, doi:10.1175/1520-0442(1992)005<0525:TSOAPO>2.0.CO;2.

Indeje, M., F. H. M. Semazzi, and L. J. Ogallo, 2000: ENSO signals in East African rainfall seasons. *Int. J. Climatol.*, **20**, 19–46, doi:10.1002/(SICI)1097-0088(200001)20:1<19::AID-JOC449>3.0.CO;2-0.

Kiladis, G. N., and H. F. Diaz, 1989: Global climatic anomalies associated with extremes in the Southern Oscillation. *J. Climate*, **2**, 1069–1090, doi:10.1175/1520-0442(1989)002,1069:GCAAWE.2.0.CO;2.

Kummerow, C., W. Barnes, T. Kozu, J. Shiue, and J. Simpson, 1998: The Tropical Rainfall Measuring Mission (TRMM) sensor package. *J. Atmos. Oceanic Technol.*, **15**, 809–817, doi:10.1175/1520-0426(1998)015<0809:TTRMMT>2.0.CO;2.

Liebmann, B., and C.A. Smith, 1996: Description of a complete (interpolated) outgoing longwave radiation dataset. *Bull. Amer. Meteor. Soc.*, **77**, 1275–1277.

——, and J. A. Marengo, 2001: Interannual variability of the rainy season and rainfall in the Brazilian Amazon basin. *J. Climate*, **14**, 4308–4318, doi:10.1175/1520-0442(2001)014<4308:IVOTRS>2.0.CO;2.

Liebmann, B., I. Bladé, G. N. Kiladis, L. M. V. Carvalho, G. B. Senay, D. Allured, S. Leroux, and C. Funk, 2012: Seasonality of African precipitation from 1996 to 2009. *J. Climate*, **25**, 4304–4322, doi:10.1175/JCLI-D-11-00157.1.

——, and Coauthors, 2014: Understanding recent eastern Horn of Africa rainfall and change. *J. Climate*, **27**, 8630–8645, doi:10.1175/JCLI-D-13-00714.1.

Lott, F. C., N. Christidis, and P. A. Stott, 2013: Can the 2011 East African drought be attributed to human-induced climate change? *Geophys. Res. Lett.*, **40**, 1177–1181, doi:10.1002/grl.50235.

Lyon, B., 2014: Seasonal drought in the Greater Horn of Africa and its recent increase during the March–May long rains. *J. Climate*, **27**, 7953–7975, doi:10.1175/JCLI-D-13-00459.1.

——, and D. G. DeWitt, 2012: A recent and abrupt decline in the East African long rains. *Geophys. Res. Lett.*, **39**, L02702, doi:10.1029/2011GL050337.

——, A. Barnston, and D. DeWitt, 2014: Tropical Pacific forcing of a 1998–99 climate shift: Observational analysis and climate model results for the boreal spring season. *Climate Dyn.*, **43**, 893–909, doi:10.1007/s00382-013-1891-9.

Maidment, R. I., R. P. Allan, and E. Black, 2015: Recent observed and simulated changes in precipitation over Africa. *Geophys. Res. Lett.*, **42**, 8155–8164, doi:10.1002/2015GL065765.

Maltima, J. M., and Coauthors, 2009: The linkages between land use change, land degradation and biodiversity across East Africa. *African J. Environ. Sci. Tech.*, **3**, 310–325.

Mason, S. J., and L. Goddard, 2001: Probabilistic precipitation anomalies associated with ENSO. *Bull. Amer. Meteor. Soc.*, **82**, 619–638, doi:10.1175/1520-0477(2001)082,0619:PPAAWE.2.3.CO;2.

Mati, B. M., 2005. Overview of water and soil nutrient management under smallholder rain-fed agriculture in East Africa. International Water Management Institute Working Paper 105, 94 pp. [Available online at http://ageconsearch.umn.edu/bitstream/92406/2/WOR105.pdf.]

McCreary, J. P., P. K. Kundu, and R. Molinari, 1993: A numerical investigation of dynamics, thermodynamics and mixed-layer processes in the Indian Ocean. *Prog. Oceanogr.*, **31**, 181–244, doi:10.1016/0079-6611(93)90002-U.

Nicholson, S. E., 1996: A review of climate dynamics and climate variability in eastern Africa. *The Limnology, Climatology and Paleoclimatology of the East African Lakes*, T. C. Johnson and E. O. Odada, Eds., Gordon and Breach, 25–56.

——, and D. Entekhabi, 1987: Rainfall variability in equatorial and southern Africa: Relationships with sea surface temperatures along the southwestern coast of Africa. *J. Climate Appl. Meteor.*, **26**, 561–578, doi:10.1175/1520-0450(1987)026<0561:RVIEAS>2.0.CO;2.

Ogallo, L. J., J. E. Janowiak, and M. S. Halpert, 1988: Teleconnection between seasonal rainfall over East Africa and global sea surface temperature anomalies. *J. Meteor. Soc. Japan*, **66**, 807–822.

Saji, N. H., B. N. Goswami, P. N. Vinayachandran, and T. Yamagata, 1999: A dipole mode in the tropical Indian Ocean. *Nature*, **401**, 360–363.

Slingo, J., H. Spencer, B. Hoskins, P. Berrisford, and E. Black, 2005: The meteorology of the western Indian Ocean, and the influence of the East African highlands. *Philos. Trans. Roy. Soc. London*, **363A**, 25–42, doi:10.1098/rsta.2004.1473.

Tierney, J. E., C. C. Ummenhofer, and P. B. deMenocal, 2015: Past and future rainfall in the Horn of Africa. *Sci. Adv.*, **1**, e1500682, doi:10.1126/sciadv.1500682.

Verdin, J., C. Funk, G. Senay, and R. Choularton, 2005: Climate science and famine early warning. *Philos. Trans. Roy. Soc.*, **B360**, 2155–2168, doi:10.1098/rstb.2005.1754.

Webster, P. J., and J. R. Holton, 1982: Cross-equatorial response to middle-latitude forcing in a zonally varying basic state. *J. Atmos. Sci.*, **39**, 722–733, doi:10.1175/1520-0469(1982)039<0722:CERTML>2.0.CO;2.

Williams, A. P., and C. Funk, 2011: A westward extension of the warm pool leads to a westward extension of the Walker circulation, drying eastern Africa. *Climate Dyn.*, **37**, 2417–2435, doi:10.1007/s00382-010-0984-y.

Yang, W., R. Seager, M. A. Cane, and B. Lyon, 2014: The East African long rains in observations and models. *J. Climate*, **27**, 7185–7202, doi:10.1175/JCLI-D-13-00447.1.

——, ——, ——, and ——, 2015: The annual cycle of East African precipitation. *J. Climate*, **28**, 2385–2404, doi:10.1175/JCLI-D-14-00484.1.